2000-01

Enhancement of the point-spread function for imaging in scattering media by use of polarization-difference imaging

Tyo, J. Scott

Enhancement of the point-spread function for imaging in scattering media by use of polarization-difference imaging

J. Scott Tyo

Department of Electrical and Computer Engineering, U.S. Naval Postgraduate School, Monterey, California 93943

Received October 26, 1998; revised manuscript received August 31, 1999; accepted August 31, 1999

Polarization-difference (PD) imaging techniques have been demonstrated to improve the detectability of target features that are embedded in scattering media. The improved detectability occurs for both passive imaging in moderately scattering media (<5 optical depths) and active imaging in more highly scattering media. These improvements are relative to what is possible with equivalent polarization-blind, polarization-sum (PS) imaging under the same conditions. In this investigation, the point-spread functions (PSF's) for passive PS and PD imaging in single-scattering media are studied analytically, and Monte Carlo simulations are used to study the PSF's in single- and moderately multiple-scattering media. The results indicate that the PD PSF can be significantly narrower than the corresponding PS PSF, implying that better images of target features with high-spatial-frequency information can be obtained by using differential polarimetry in scattering media. Although the analysis was performed for passive imaging at moderate optical depths, the results lend insight into experiments that have been performed in more highly scattering media with active imaging methods to help mitigate the effects of multiple scattering. [S0740-3232(00)00501-9]
OCIS codes: 260.5430, 110.0110, 070.2580, 230.5440, 110.7050.

1. INTRODUCTION

The problem of intervening scatterers presents a variety of challenges to the process of imaging in applications such as atmospheric remote sensing, underwater photography, and medical imaging. Depending on the application and on the nature of the scattering medium, a number of different approaches have been developed to overcome the effects of scatterers, including time-resolved imaging,[1–3] confocal microscopy,[4] optical coherence methods,[3,4] and diffusive photon imaging.[5] Each of these techniques has its regime of utility and associated cost and complexity. More-advanced methods can be rather expensive to implement and might not be appropriate for lower-scattering regimes where simpler techniques can be useful. Furthermore, most of the strategies that have been developed for imaging in scattering media rely on active illumination, a condition that prevents their use in some remote sensing applications.

An additional class of techniques that has shown the potential to aid in the detection of targets embedded in scattering media involves sensing of the polarization properties of the radiation.[6–8] Such techniques have exploited the polarization of the incident radiation,[8] radiation scattered by the target,[7] or both[6] in order to mitigate the effects of multiple scattering. Research has shown that passive systems employing linear polarization-difference imaging (PDI) can improve the detectability of target features that introduce partial polarization into the scattered radiation when the images are obtained in random media. In addition to the benefit that can be obtained by using PDI alone, differential polarimetry is relatively easy to implement and is highly flexible, can be used with passive or active illumination, and can be combined with more-complicated techniques such as time-resolved imaging[1,9] and optical coherence methods[10] to further enhance target detectability.

It was hypothesized by Tyo *et al.*[7] that the observed benefit of PDI in resolving target features is due to an enhancement of the point-spread function (PSF) relative to the PSF of conventional imaging. The enhancement is due to the effects of multiple scattering; while multiple scattering results in blurring that degrades the conventional PSF, the same scattering also results in depolarization. Because differential polarimetric techniques such as PDI are less sensitive to this depolarized radiation than are polarization-blind methods, they are not affected as adversely by the multiply scattered light. In related research, Harris[11] demonstrated that the degree of polarization of a normally incident, linearly polarized plane wave decreases as a function of distance of propagation into a slab of random medium. Kuga and Ishimaru[12,13] studied the intensity-only modulation transfer function (MTF—equivalent to PSF[14]) in scattering media, and Ma and Ishimaru[15] studied the intensity-only MTF of an arbitrarily polarized plane wave in optically scattering media composed of a suspension of spherical scatterers in water. Although the propagation of polarized radiation in random media has been treated, none of these studies examined the effects of polarization discrimination at the receiver on the MTF. Since researchers have shown that the MTF for radar images of the sea surface are polarization dependent[16,17] and that the optical transfer function of a lensing system with polarization masks is dependent on the polarization state of the incident light,[18] there is reason to believe that the PSF's of random media may be dependent on polarization properties of the incident

and/or the scattered radiation, as well as on the polarization-discrimination technique used to analyze the received signal. Preliminary numerical[19] and experimental[9,20] studies have indicated that the above hypothesis concerning a narrowing of the PSF may indeed be valid. In this paper the shape of the PSF's for polarization-sum (PS—conventional imaging[7]) and polarization-difference (PD) imaging are compared in a random medium, and it is shown that the PD PSF is indeed narrower than the PS PSF. The narrowing of the PSF allows for improved resolution of certain target features in PD images obtained in a scattering medium[14] relative to what is possible by use of conventional PS imaging alone. This result is in agreement with already reported experimental investigations of PDI in scattering media.[7] In Section 2 of this paper a simplified analytic model is presented that provides insight into the problem in a single-scattering medium. In Section 3 the analysis is extended by Monte Carlo methods to scattering regimes comparable to those studied previously.[7,19,21–23] In Section 4 the results are summarized and their impact on experimental studies is discussed.

2. ANALYTIC FORMULATION

In this section the PSF of an optical imaging system observing a linearly polarized point source through a thin scattering medium is studied. For mathematical brevity a simplified, canonical imaging system is analyzed, although the results obtained can be generalized to more-complex imaging configurations in a straightforward manner. Using the single-scattering approximation[24] (SSA) for the scattering medium in conjunction with a Fourier optics[14] analysis of the imaging system, an expression for the PSF of an ideal imaging system *plus* a scattering medium will be derived. The potential for Fourier plane spatial filtering is included in the formulation (but not explicitly studied), since such a technique has been demonstrated to improve image quality in scattering media under certain conditions.[25,26]

The experimental setup analyzed in this section is depicted in Fig. 1. An elemental dipole source is located at the object plane of a two-lens imaging system. In the far field of the source, the dipole appears linearly polarized regardless of the direction of observation. This type of source relates to the problem of imaging in scattering media in that light scattered from a particular location on a target will have a polarization state that can be approximated by the incoherent addition of completely polarized point sources. The analysis presented here is most relevant to the imaging of self-luminous point sources embedded in scattering media such as those studied in Refs. 9 and 20. For images of targets that are passively or actively illuminated by an external source, direct scattering from the source into the receiver must also be considered in order for one to be able to predict the actual image. The source–receiver interaction is a problem that depends on the specific parameters of the optical setup and is therefore omitted from this study so that we can concentrate on the blurring and depolarization that occur after scattering from the target that is being imaged.

The optical system considered here is composed of two identical lenses separated by twice the focal length f. The point source is located in the object plane (O) a distance f in front of the first lens. A Fourier plane spatial filter can be included in the intermediate plane. The transfer function of this filter is denoted as $G(x_a, z_a)$ and serves to alter the Fourier spectrum of the amplitude distribution in the object plane.[14,25,26] The apertures of the lenses are not considered explicitly, since they can be projected onto the intermediate plane and included in the construction of the filter $G(x_a, z_a)$.[27] The image is formed at the image plane a distance f behind the second lens. In general, the placement of the optical elements

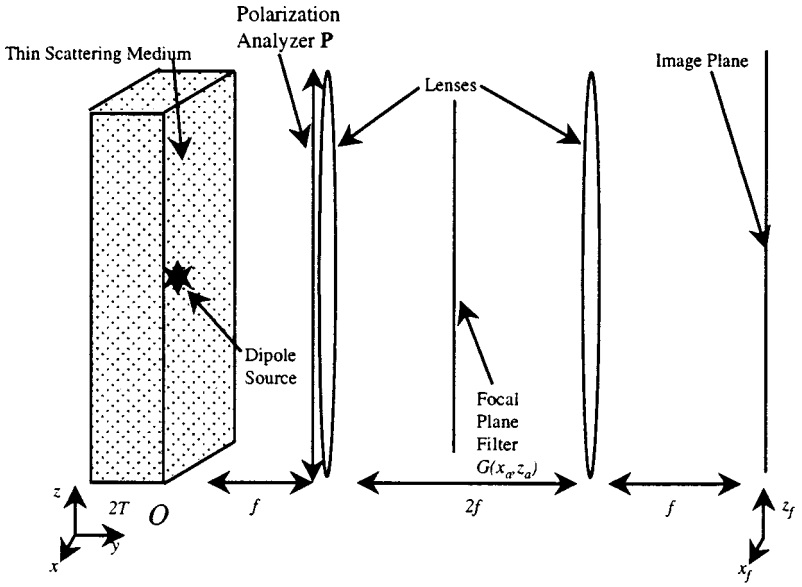

Fig. 1. PSF geometry considered. An elemental dipole is parallel to the z axis is located at the origin in a scattering medium of thickness $2T$ in the y direction. The medium is infinite in the x and z directions. The radiation is captured by an imaging system made up of two lenses separated by twice the focal length f. The first lens is f from the dipole and the second lens is f from the image plane. A focal-plane filter can be included at the Fourier transform plane between the two lenses. For simplicity, $T \ll f$ is assumed.

can be changed, thereby allowing the imaging system to focus outside the plane O; however, such an alteration will change the effective transfer function of the spatial filter $G(x_a, z_a)$. The object plane is located at the center of an infinite slab of scattering medium of thickness $2T$ in the direction of propagation. The medium is composed of identical scatterers uniformly distributed throughout the slab with concentration ρ. A polarization analyzer with electric field transmission matrix $\mathbf{P}$ is placed in front of the first lens to allow for investigation of a PDI system.

When employing the SSA, one assumes that the particles composing the scattering medium are noninteracting, i.e., that the incident field at the location $\vec{\mathbf{r}}_n$ of the nth scatterer is the field due only to the dipole source (Born approximation).[11,24] It is further assumed that each scatterer is in the far field of the dipole source and that the expanding spherical phase front that is incident on each scatterer is approximated locally as a plane wave. The scattering geometry for a single scatterer is depicted in Fig. 2. The dipole source is taken at the origin with current directed along $\hat{\mathbf{z}}$. At the position $\vec{\mathbf{r}}_n$ in the far field of the dipole, the field is

$$\vec{\mathbf{E}}(\vec{\mathbf{r}}_n) = A\,\frac{\exp(ikr)}{r}\sin\theta\,\hat{\boldsymbol{\theta}}, \tag{1}$$

where k is the propagation constant,[28] the time dependence $\exp(-i\varpi t)$ has been assumed and suppressed, and the constant A describes the specific features of the dipole source under investigation. To find the effect of the nth scatterer on the final image, one must take the scattering amplitude $\underline{f}(\hat{\mathbf{s}}, \hat{\mathbf{s}}')$ into account, where $\hat{\mathbf{s}}'$ is the incident direction, $\hat{\mathbf{s}}$ is the scattered direction, and $\underline{f}(\hat{\mathbf{s}}, \hat{\mathbf{s}}')$ describes the scattering of a plane wave from $\hat{\mathbf{s}}'$ into $\hat{\mathbf{s}}$.[24] The scattered field takes the form

$$\mathbf{E}_{\mathrm{sc}}(\hat{\mathbf{s}}) = \underline{f}(\hat{\mathbf{s}},\hat{\mathbf{s}}')\vec{\mathbf{E}}_{\mathrm{in}}(\hat{\mathbf{s}}'), \tag{2}$$

where $\vec{\mathbf{E}}_{\mathrm{in}}(\hat{\mathbf{s}}')$ is the incident field in the direction $\hat{\mathbf{s}}'$ defined by Eq. (1).[29] In general, the functional form of the scattering amplitude will depend on the choice of coordinate system for the scattering event and on the physical structure of the individual scatterers. The cases of Rayleigh- and Mie-scattering[24,30] particles are considered below. Regardless of the specific scattering function, the scattered field in the far field of the scatterer takes on the form of a spherical wave expanding about the scatterer, so the effect of the nth scatterer can be considered by analyzing a point source with the appropriate relative amplitude at the location $\vec{\mathbf{r}}_n$ in the imaging system depicted in Fig. 1.

In the study of the imaging properties of the system, the paraxial approximation is employed.[14] The paraxial approximation assumes that all radiation that contributes to the image propagates near normally to the system aperture, i.e., is near normal to the polarization analyzer, so that $|\hat{\mathbf{R}}\cdot\hat{\mathbf{n}}| \cong 1$, where the unit vector $\hat{\mathbf{R}}$ indicates the direction that connects the scatterer to any particular location on the aperture and $\hat{\mathbf{n}}$ is the surface normal of the aperture at the location corresponding to $\hat{\mathbf{R}}$. This approximation fixes the scattered direction $\hat{\mathbf{s}}$ in Eq. (2) as the $\hat{\mathbf{y}}$ direction, as shown in Figs. 1 and 2.

To determine the effect of the scatterers on the final image, the following steps are carried out: (1) The image of a single scatterer located at $\mathbf{r}_n$ is found; (2) the image from a single realization of the ensemble of potential scatterer arrangements is determined; (3) the expectation of the image is considered over the ensemble of all possible realizations of scatterer arrangements. This procedure assumes that expectations over time, space, and ensemble are equivalent.[11]

From Fourier optics, the field at the image plane that is due to a point source at $\mathbf{r}_n$ is[14]

$$\begin{aligned}\vec{\mathbf{E}}_f^{(n)}(x_f, z_f) = {} & \frac{B\exp[ik(4f - y_n)]}{(\lambda f)^2}\int\!\!\int_O \mathbf{P}\vec{\mathbf{E}}_{\mathrm{sc}}^{(n)}(\hat{\mathbf{y}})\kappa^2 \\ & \times \delta(x_o - x_n)\delta(z_o - z_n)\int\!\!\int_A G(x_a, z_a) \\ & \times \exp\left[i\frac{\pi}{\lambda f}\frac{y_n}{f}(x_a^2 + z_a^2)\right] \\ & \times \exp\left\{-i\frac{2\pi}{\lambda f}[x_a(x_o + x_f) \right. \\ & \left. + z_a(z_o + z_f)]\right\}\mathrm{d}x_a\mathrm{d}z_a\mathrm{d}x_o\mathrm{d}z_o,\end{aligned} \tag{3}$$

where $\vec{\mathbf{E}}_f^{(n)}$ is the field at the image plane that is due to the nth scatterer, $\delta(\cdot)$ is the Dirac delta function, κ is a constant introduced to compensate for the units of the Dirac delta functions, $\mathbf{P}$ is the transmission matrix of the polarization analyzer in front of the first lens in Fig. 1, B is a constant that is the same for all scatterers that takes into account any attenuation within the system, and $\vec{\mathbf{E}}_{\mathrm{sc}}^{(n)}(\hat{\mathbf{y}})$ is the scattered field from the nth scatterer in the $\hat{\mathbf{y}}$ direction as computed with Eq. (2). The subscripts O and o represent the object plane, A and a represent the intermediate plane between the two lenses, and F and f represent the image plane. Equation (3) can be simplified as

$$\begin{aligned}\vec{\mathbf{E}}_f^{(n)}(x_f, z_f) = {} & \frac{B\kappa^2\exp[ik(4f - y_n)]}{(\lambda f)^2}\mathbf{P}\vec{\mathbf{E}}_{\mathrm{sc}}^{(n)} \\ & \times \mathfrak{F}_2\left\{G(x_a, z_a) \right. \\ & \left. \times \exp\left[i\frac{\pi}{\lambda f}\frac{y_n}{f}(x_a^2 + z_a^2)\right]\right\}\Bigg|_{f_x, f_z},\end{aligned}$$

$$f_x = \frac{x_n + x_f}{\lambda f}; \quad f_z = \frac{z_n + z_f}{\lambda f}, \tag{4}$$

where $\mathfrak{F}_2\{X(x, z)\}|_{f_x, f_z}$ is the two-dimensional Fourier transform of the spatial function $X(x, z)$ evaluated at the values f_x and f_z of the spatial-frequency variables. To find the field that is due to just the scatterers for a single realization of scatterer arrangement, Eq. (4) is summed over the entire volume

$$\vec{\mathbf{E}}_f(x_f, z_f) = \sum_{n=1}^{N}\vec{\mathbf{E}}_f^{(n)}(x_f, z_f), \tag{5}$$

where N is the number of scatterers. To find the ensemble average, one should sum over all possible configurations of the point scatterers. However, since the image is composed of the *intensity* distribution, and since the positions of the scatterers are assumed to fluctuate independently, the expectation operation results in the sum of field amplitudes in Eqs. (5) being replaced by an integral of intensities that are due to uniformly distributed scatterers[24]:

$$|\vec{\mathbf{E}}_f(x_f, z_f)|^2 = \int_V |\vec{\mathbf{E}}_f(x_f, z_f; x_o, y_o, z_o)|^2 \rho \mathrm{d}x_o \mathrm{d}y_o \mathrm{d}z_o, \tag{6}$$

where V is the volume of the scattering slab, $\vec{\mathbf{E}}_f(x_f, z_f; x_o, y_o, z_o)$ is the field at location (x_f, z_f) in the image plane due to the scatterer at location (x_o, y_o, z_o), and

$$\int_V \rho \mathrm{d}x_o \mathrm{d}y_o \mathrm{d}z_o = N. \tag{7}$$

The integral in Eq. (6) represents an expectation over an ensemble of uniformly distributed scatterers and gives the portion of the incoherent PSF that is due to the scatterers only. The portion of the PSF that is due to the dipole source will be that of a diffraction-limited imaging system and should be included to obtain the complete PSF.

A. Rayleigh Scatterers

The scattered field from objects that are small compared with the wavelength of the incident radiation has a dipole-like radiation pattern in the far field.[24] Referring to Fig. 2, the scatterer at position $\vec{\mathbf{r}}_n$ sees an approximate plane wave propagating in the $\hat{\mathbf{r}}$ direction polarized in the $\hat{\boldsymbol{\theta}}$ direction.[31] A primed coordinate system is defined at the nth scatterer with $\hat{\mathbf{z}}'$ along the direction of polarization of incident radiation ($\hat{\boldsymbol{\theta}}$) and $\hat{\mathbf{y}}'$ along the direction of propagation of the incident radiation ($\hat{\mathbf{r}}$). The scattered field from the nth scatterer observed at a distance R from the scatterer along the direction $\hat{\mathbf{s}}$ is

$$\vec{\mathbf{E}}_{\mathrm{sc}}^{(n)}(\hat{\mathbf{s}}) = |\vec{\mathbf{E}}_{\mathrm{in}}(\vec{\mathbf{r}}_n)| \exp(ik|\vec{\mathbf{r}}_n|) \frac{C}{R} \exp(ikR) \sin\theta' \, \hat{\boldsymbol{\theta}}', \tag{8}$$

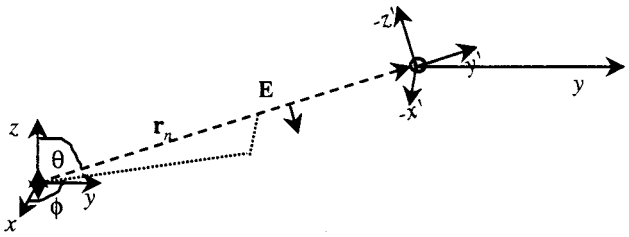

Fig. 2. Geometry for a single scatterer. The nth scatterer is located at the position $\mathbf{r}_n$. The polarization is in the θ direction. At the scatterer the primed coordinates are used to solve for the scattering amplitude with Rayleigh or Mie theory. It is assumed that all scatterers in the medium are identical and that all scatterers are in the far field of the dipole source. In the SSA it is further assumed that all the scatterers are also noninteracting.

where θ' is the polar angle defined with respect to the primed coordinate system. The scale factor C describes the specific scattering geometry and is identical for all scatterers. The angle θ' is expressed in terms of the angles θ and ϕ of the unprimed coordinate system: $\hat{\mathbf{s}} = \hat{\mathbf{y}}$ and $\hat{\mathbf{s}} \cdot \hat{\mathbf{z}}' = \cos\theta' = \cos\theta \sin\phi$. Furthermore,

$$\begin{aligned}\hat{\boldsymbol{\theta}}' &= \frac{(\hat{\mathbf{z}}' \times \hat{\mathbf{r}}') \times \hat{\mathbf{r}}'}{|(\hat{\mathbf{z}}' \times \hat{\mathbf{r}}') \times \hat{\mathbf{r}}'|} = \frac{1}{(1 - \cos^2\theta \sin^2\phi)^{1/2}} \\ &\quad \times [-\cos\theta \cos\phi \hat{\mathbf{x}} + \sin\theta \hat{\mathbf{z}}] \\ &= \frac{1}{\sin\theta'} [-\cos\theta \cos\phi \hat{\mathbf{x}} + \sin\theta \hat{\mathbf{z}}],\end{aligned} \tag{9}$$

so that

$$\begin{aligned}\vec{\mathbf{E}}_{\mathrm{sc}}^{(n)}(\hat{\mathbf{s}}) &= |\vec{\mathbf{E}}_{\mathrm{in}}(\vec{\mathbf{r}}_n)| \exp(ik|\vec{\mathbf{r}}_n|) \frac{C}{R} \exp(ikR) \\ &\quad \times [-\cos\theta \cos\phi \hat{\mathbf{x}} + \sin\theta \hat{\mathbf{z}}].\end{aligned} \tag{10}$$

If it is assumed that the thickness of the scattering slab is small with respect to the focal length ($T \ll f$) and that the imaging system is ideal [$G(x_a, z_a) = 1$], then Eq. (4) reduces to

$$\begin{aligned}\vec{\mathbf{E}}_f^{(n)}(x_f, z_f) &= \frac{B\kappa^2}{(\lambda f)^2} \exp[ik(4f - y_n)] \mathbf{P} \vec{\mathbf{E}}_{\mathrm{sc}}^{(n)}(\hat{\mathbf{s}}) \delta(f_x) \delta(f_z) \\ &\approx B\kappa^2 \mathbf{P} \vec{\mathbf{E}}_{\mathrm{sc}}^{(n)}(\hat{\mathbf{s}}) \delta(x_f + x_n) \delta(z_f + z_n).\end{aligned} \tag{11}$$

Substituting Eqs. (1), (10), and (11) into Eq. (6) yields[32]

$$\begin{aligned}|\vec{\mathbf{E}}_f(x_f, z_f)|^2 &= \int_{y_o=-T}^{T} \rho |\mathbf{P} \vec{\mathbf{E}}(x_f, z_f; -x_f, y_o, -z_f)|^2 \mathrm{d}y_o \\ &= \left(\frac{ABC\kappa}{R}\right)^2 \int_{y_o=-T}^{T} \frac{\rho \sin^2\theta}{r^2} |\mathbf{P}[-\cos\theta \cos\phi \hat{\mathbf{x}} \\ &\quad + \sin\theta \hat{\mathbf{z}}]|^2 \mathrm{d}y_o,\end{aligned} \tag{12}$$

where the position (r, θ, ϕ) describes the point $(x_o = -x_f, y_o, z_o = -z_f)$ in spherical coordinates with respect to the unprimed coordinate system. Notice that the intensity at location (x_f, z_f) in the image plane is due to the point scatterers located at $(x_o = -x_f, -T \leqslant y_o \leqslant T, z_o = -z_f)$ in the object plane. Equation (12) contains an apparent contradiction because the integral can be taken through the origin, but it was assumed above that all scatterers are in the far field of the dipole source. This contradiction can be resolved by making the density function ρ a function of the radius $r = (x_o^2 + y_o^2 + z_o^2)^{1/2}$ by

$$\rho \rightarrow \rho(r) = \begin{cases} 0, & r < r_0 \\ \rho_0, & \text{otherwise} \end{cases}, \tag{13}$$

where ρ_0 is chosen so that the normalizing relationship in Eq. (7) still holds. Practically, the vanishingly small portion of scatterers in the near field of the dipole does not contribute significantly to the imaged intensity.

Changing the functional dependence of ρ will allow evaluation of Eq. (12) at all locations but provides little additional insight into the shape of the PSF. For that reason, Eq. (12) will be evaluated as is, and the singularity will be dealt with subsequently to aid in interpreting

the results. When the standard spherical → Cartesian transformation is used, Eq. (12) can be converted to an algebraic expression in y_o and evaluated by using integral tables or a suitable symbolic package (e.g., Mathematica, v2.2).

If the analyzer given by $\mathbf{P}$ allows only the $\hat{\mathbf{x}}$ component of the radiation to pass, then

$$|\tilde{\mathbf{E}}_f^{\mathbf{x}}(x_f, z_f)|^2 = \rho\left(\frac{ABC\kappa}{R}\right)^2\left[\frac{-Tz_f^4}{2\nu_f^2(T^2+\nu_f^2)^2} + \frac{Tz_f^2(4x_f^2+z_f^2)}{4\nu_f^4(T^2+\nu_f^2)} + \frac{z_f^2(4x_f^2+z_f^2)\tan^{-1}\left(\frac{T}{\nu_f}\right)}{4\nu_f^5}\right], \quad (14)$$

where $\nu_f^2 = x_f^2 + z_f^2$ is equivalent to the square of the two-dimensional radius with respect to the point ($x_f = 0$, $z_f = 0$) in the image plane. Likewise, if $\mathbf{P}$ allows only the $\hat{\mathbf{z}}$ component to pass, then

$$|\tilde{\mathbf{E}}_f^{\mathbf{z}}(x_f, z_f)|^2 = \rho\left(\frac{ABC\kappa}{R}\right)^2\left[\frac{Tz_f^4}{2\nu_f^2(T^2+\nu_f^2)^2} - \frac{Tz_f^2(8x_f^2+5z_f^2)}{4\nu_f^4(T^2+\nu_f^2)} + \frac{(8x_f^4+8x_f^2z_f^2+3z_f^4)\tan^{-1}\left(\frac{T}{\nu_f}\right)}{4\nu_f^5}\right]. \quad (15)$$

In the limit $\nu_f \gg T$, the integrand in Eq. (12) is approximately constant, and Eqs. (14) and (15) are proportional to $\sin^2\theta\cos^2\theta/\nu_f^2$ and $\sin^4\theta/\nu_f^2$, respectively. If

$$\tan^{-1}\left(\frac{T}{\nu_f}\right) \cong \frac{T}{\nu_f}, \quad (16)$$

the above condition is satisfied and the two equations reduce to the simpler form.

In this investigation the PSF's for PS and PD imaging are compared[33]:

$$|\tilde{\mathbf{E}}_f^{\mathrm{PS}}(x_f, z_f)|^2 = |\tilde{\mathbf{E}}_f^{\mathbf{x}}(x_f, z_f)|^2 + |\tilde{\mathbf{E}}_f^{\mathbf{z}}(x_f, z_f)|^2,$$
$$|\tilde{\mathbf{E}}_f^{\mathrm{PD}}(x_f, z_f)|^2 = |\tilde{\mathbf{E}}_f^{\mathbf{x}}(x_f, z_f)|^2 - |\tilde{\mathbf{E}}_f^{\mathbf{z}}(x_f, z_f)|^2. \quad (17)$$

The distributions of the portion of the PSF that is due to the scatterers is depicted in Fig. 3. As was mentioned earlier, the factor of $1/r^2$ in Eq. (12) causes a singularity at the origin. The most interesting features of the PSF's can be better visualized if the radial variation is suppressed in displaying the PSF's, resulting in an angular description of the portion of the PSF's that is due to the scatterers. The results obtained by Eqs. (17) are multiplied by ν_f^2 and are plotted again in Fig. 4.

As demonstrated in Figs. 3 and 4, the PD PSF shows a narrowing in the angular domain relative to the PSF of intensity-only imaging. The 3-dB azimuthal width of the PS PSF is 90°, and the 3-dB azimuthal width of the PD PSF is approximately 51°. Further generalization to rigorous multiple-scattering theory causes the single-polarization PSF's given in Eqs. (14) and (15) to become more similar, thus making the portion of the PD PSF that is due to scatterers decrease further, as is demonstrated below with Monte Carlo simulations.

B. Mie Scatterers

Many realistic scattering media can be approximated by using a scattering amplitude derived from Mie theory.[24,30,34,35] With the Mie-scattering amplitude used

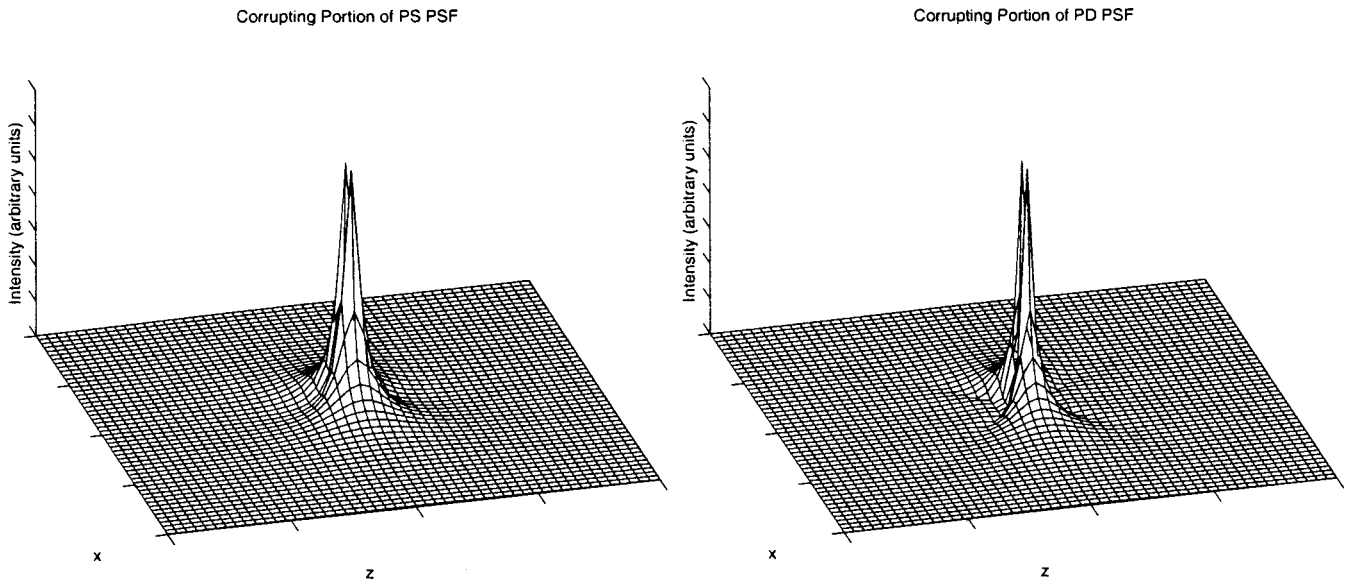

Fig. 3. Corrupting portions of the PS and PD PSF's for a medium of Rayleigh scatterers calculated by using the SSA. These plots show that the PD PSF is narrower than the PS PSF in such a medium.

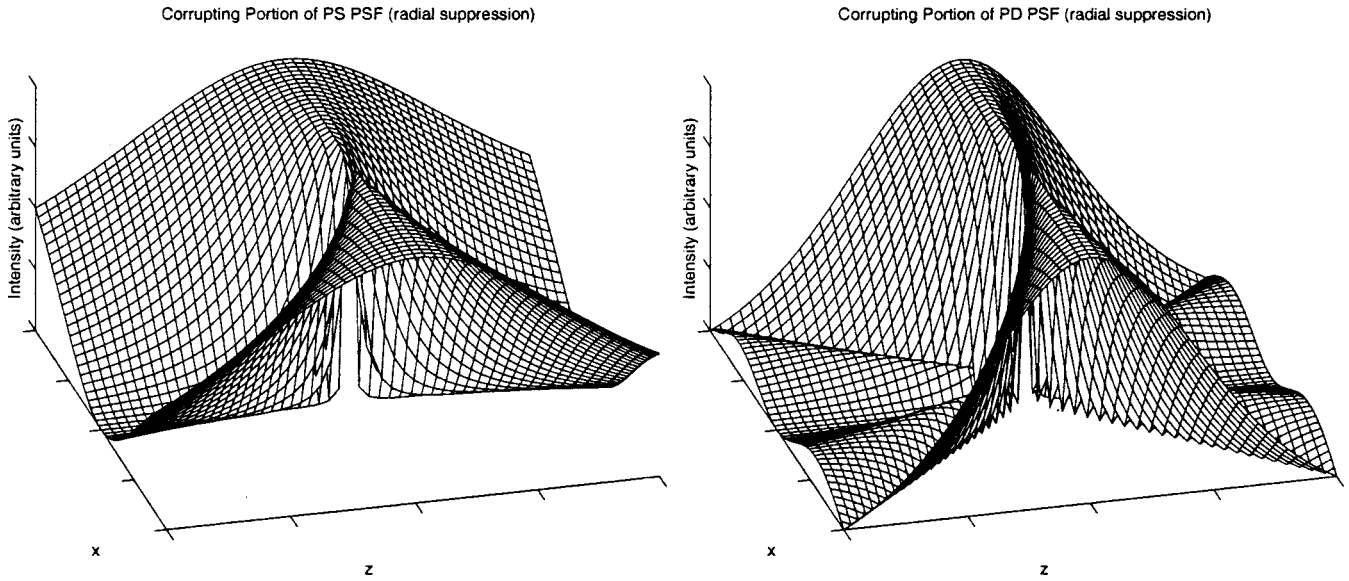

Fig. 4. Corrupting portions of the PS and PD PSF's presented in Fig. 3 with radial variation suppressed by multiplying by ν_f^2. With this presentation scheme the narrowing with respect to the x axis is more pronounced. The null can now clearly be seen at 45°. The actual PD PSF has a zero crossing at 45°, but the magnitude of the PD PSF is presented in this figure (as well as in Fig. 3).

in Eq. (2), the integral in Eq. (6) can be quite difficult to evaluate. Some qualitative insight into the problem can be gleaned by examining the simpler problem where all the scatterers exist in the same plane as the dipole source, i.e., the object plane O, i.e., the limit of a thin medium, where

$$|\tilde{\mathbf{E}}_f^{\mathbf{x}}(x_f, z_f)|^2 \propto \frac{1}{r^2}\sin^2\theta\cos^2\theta\cos^2\phi,$$

$$|\tilde{\mathbf{E}}_f^{\mathbf{z}}(x_f, z_f)|^2 \propto \frac{1}{r^2}\sin^4\theta, \tag{18}$$

where (r, θ, ϕ) once again describes the position $(x_o = -x_f, y_o = 0, z_o = z_f)$ with respect to the dipole source at the origin. Note that relation (18) is virtually identical to the limiting form of Eq. (12) given above, so the shapes of the PSF's for a single-scattering medium of Mie scatterers is similar to the ones depicted in Figs. 3 and 4.

In review, the SSA analysis makes four predictionsabout the PSF's for PD and PS images of an elemental dipole oriented in the z direction located at the origin in a thin, weak Rayleigh medium: (1) The corrupting portions of the PD and PS PSF's are zero along the z axis (parallel to the dipole). (2) The corrupting portions of the PD and PS PSF's are maximum and equal along the x direction (perpendicular to the dipole) and fall off at the same rate. (3) The PD PSF has a null in the direction 45° from the orientation of the dipole; the PS PSF has no such null. (4) The 3-dB azimuthal width of the PS PSF is 90° and the 3-dB width of the PD PSF is approximately 51°, yielding an azimuthal narrowing of the PSF by 43%.

The above analysis employing the SSA is applicable over an extremely limited range of experimental parameters.[24] If the analysis is generalized further to include multiple-scattering effects, it will be difficult to obtain closed-form solutions for the imaged intensity distributions, and numerical analyses must be applied. Even though the above analysis is simple, it may provide some insights into previous experimental studies that employed polarization sensitivity to improve image contrast and resolution at moderate optical thicknesses (0–10 transport mean free paths).[7,21–23] The results also are applicable to time-resolved polarization imaging where improved two-point resolution was observed.[9,20] Even though the time-resolved imaging was performed at much greater optical thicknesses (>10 transport mean free paths), the use of time gating greatly reduces the number of multiply scattered photons that degrade the final image, thereby making the comparison with the results presented in this paper possible. Below, a Monte Carlo simulation is used to verify the four predictions made by SSA analysis and to extend the concept of a PD PSF into the multiple-scattering regime at effective distances similar to those studied experimentally in, for example, Refs. 7 and 21–23.

3. MONTE CARLO SIMULATION

A Monte Carlo code is a probabilistic code used widely in astronomy, astrophysics, particle physics, optics, imaging, chemistry, etc.[36,37] For an optical problem such as the one dealt with in this section, a Monte Carlo code tracks photon lifetimes from the time the photons are created by the source until they pass out of the system. The code is completely probabilistic, so the most important aspect of the simulation lies in determining the underlying probability density functions (PDFs) that govern the emission and scattering of photons and generating random variables with these PDFs. In this study the PDFs for direction of scatter are derived from the corresponding classical scattering functions for Rayleigh and Mie particles.

Briefly, the Monte Carlo code utilized here models a short-dipole source located inside an optically scattering medium of thickness $2T$ (T is varied) being imaged by the ideal imaging system depicted in Fig. 1. Three random numbers are generated at the emission of each photon, and these numbers determine the starting direction (θ, ϕ) in accordance with the dipole radiation pattern and the distance traveled before the initial scattering event. Values for the random variables are determined by uniformly sampling the cumulative density functions.[36] After each scattering event, two more random numbers are generated to determine the direction of scatter. Once the direction of scatter is known, the polarization state of the scattered photon is calculated from the classical equations. A third random number is generated to give the distance traveled to the next scattering event. This process is continued until the photon exits the medium. The paraxial approximation employed above dictates that only radiation traveling approximately parallel to the y axis (Fig. 2) is imaged. An acceptance solid angle is defined for the optical system, and photons leaving the front face of the medium ($y = T$) within this acceptance solid angle are passed through a polarization analyzer and are then imaged. From the resulting spatial photon distributions at the image plane, the PS and PD PSF's are determined.

A. Single-Scattering Medium

In Fig. 5 the corrupting portion of the PSF's for PS and PD images of a dipole source located at the center of a random medium of Rayleigh scatterers of total thickness is equal to 0.4 attenuation lengths. In this simulation almost 80% of the imaged photons exit the medium without having been scattered, and 17% of the imaged photons were scattered only once. The remaining 3% were scattered fewer than five times. On average, there were 0.26 scattering events per photon, so that the SSA is applicable to this example.[24] It should be noted that the plots in Fig. 5 are the corrupting portions only, and the radial variations that were suppressed above are obviously accounted for in the Monte Carlo code. The peak at the origin is due to forward-scattered photons, and the additional peak due to unscattered photons that is not presented is approximately 30 times greater than the peak shown in the figure. These unscattered photons are polarized in the z direction because they are paraxial and have retained the initial polarization state ($\hat{\boldsymbol{\theta}}$), so their contributions to the PS and PD images are identical.[38] It is important to point out that at this small optical thickness, conventional imaging techniques can still resolve certain image features. However, it has been shown that even at small optical thicknesses, polarization discrimination can enhance contrast, thereby improving target detectability.[7,22,23]

Investigation of Figs. 5 and 6 indicates that the corrupting portion of the PD PSF is not only narrower than the corrupting portion of the PS PSF, but it is also lower in absolute intensity. This lowering in absolute intensity is due to the finite-acceptance solid angle in the Monte Carlo code and, in part, to multiple-scattering effects that were not accounted for in the SSA analysis above. The multiply scattered radiation will tend to be more depolarized,[11] and unpolarized radiation is not imaged by PDI.

Figure 6 shows normalized plots of slices of the two PSF's taken parallel to the z axis (parallel to the dipole source) at different locations on the x axis. These plots are normalized so that both the PS and the PD plots have unit magnitude at the x axis. The x locations of the slices are indicated in the caption of Fig. 6. These plots demonstrate that the PD PSF is indeed narrower, as was predicted above. Because of the rectangular grid used in the Monte Carlo simulation, determination of the exact azimuthal width is difficult; however, these values can be ap-

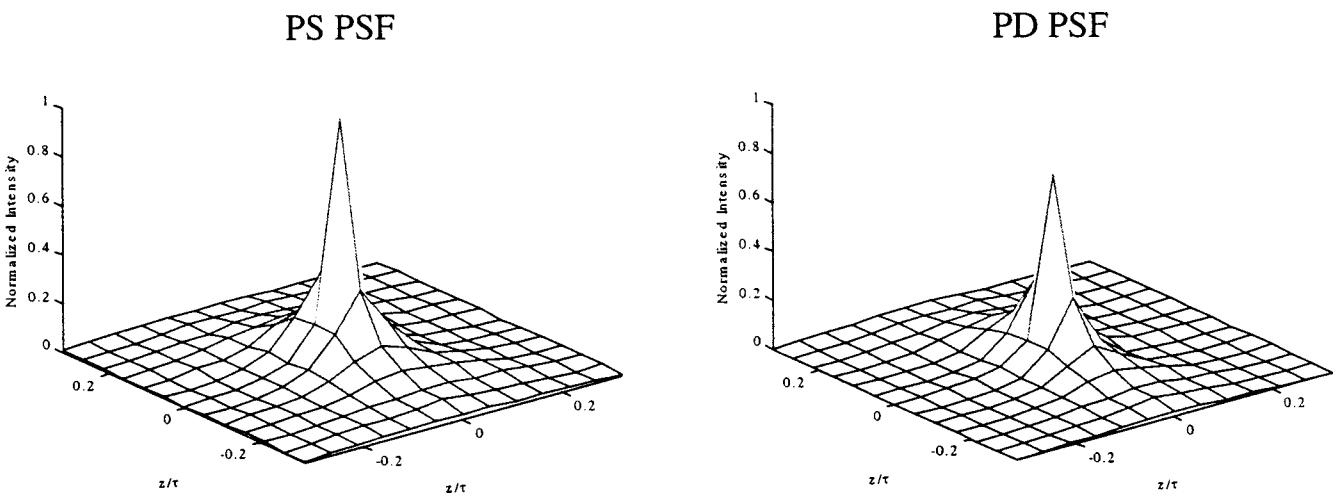

Fig. 5. Corrupting portions of the PS and PD PSF's for a medium of Rayleigh scatterers that total 0.4 attenuation lengths thick. The mean number of scattering events per measured photon was 0.26. These PSF's were obtained by Monte Carlo simulation and are meant to verify the results shown in Figs. 3 and 4. The SSA predicts that the two PSF's should have the same absolute maximum value, but as is evident above, they do not. This is due to the finite acceptance solid angle in the Monte Carlo simulation as discussed in the text. A narrowing of the PD PSF is apparent along slices taken parallel to the z axis, as was predicted by the SSA theory. This narrowing is more apparent in Fig. 6. Both PSF's are normalized to the value of the PSF for the PS image, and the two plots are presented on the same vertical scale.

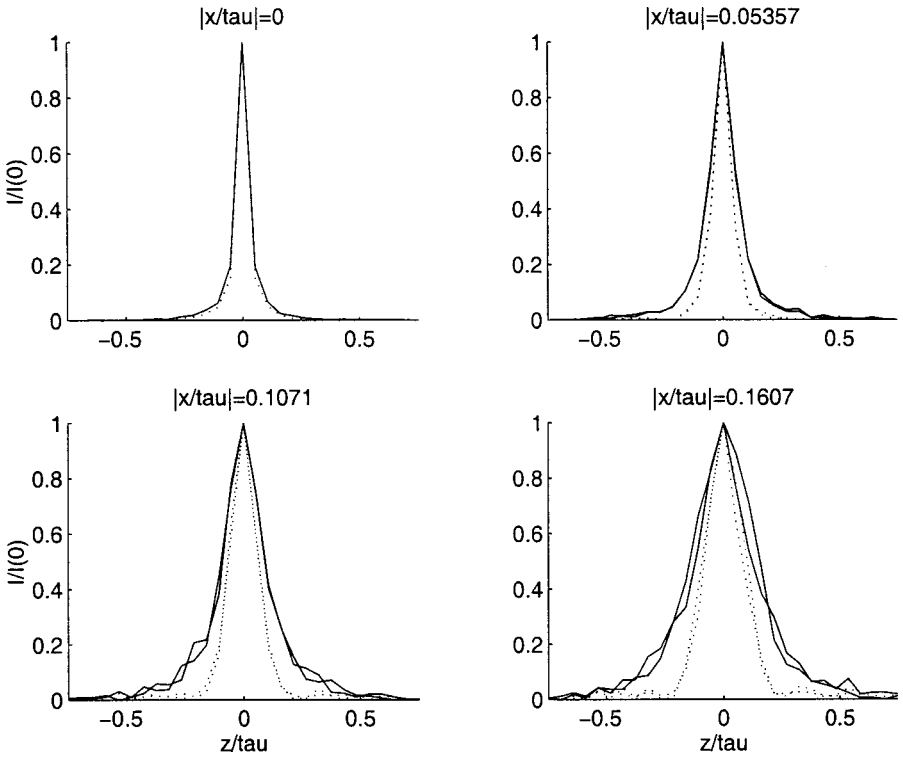

Fig. 6. Slices of the PS and PD PSF's shown in Fig. 5 taken parallel to the z axis at varying x positions given in terms of the attenuation length τ. In each of the plots for $|x/\tau| > 0$, two sets of curves are plotted that correspond to $\pm|x/\tau|$. The solid curves are slices of the PS PSF, and the dotted curves are slices of the PD PSF. All curves have been normalized to their peak values to facilitate comparison with Fig. 4. At $|x| = 0$, the PD and PS PSF's are at their narrowest point as expected, and they are approximately the same width; however, as $|x|$ increases, the width of the PS PSF parallel to the dipole increases faster than does the width of the PD PSF.

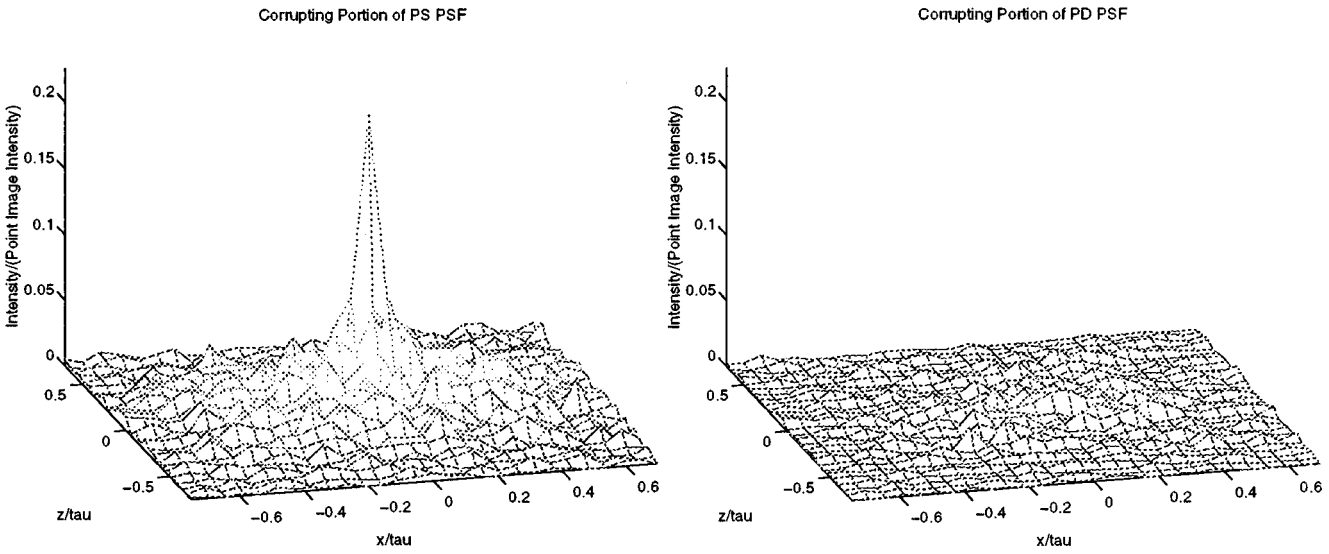

Fig. 7. Corrupting portion of the PS and PD PSF's computed, with Monte Carlo simulations for a medium of Mie scatterers that total 4 attenuation lengths thick. The mean number of scattering events per photon collected was 2.05. The Mie-scattering function used is that for spherical particles that have a radius equal to twice the wavelength of the incident radiation. The index of refraction of the sphere relative to the surrounding medium is 1.20, nearly the same as that of latex in water. The Mie-scattering function has an anisotropy factor (mean cosine) of $g = 0.8031$, which is typical of the anisotropy factor found in human tissue.[35] The point image intensity is the intensity due to unscattered light at the location of the source in the image plane. Since the medium depolarizes the radiation, the corrupting portion of the PD PSF is significantly lower than that of the PS PSF. The complete PSF is obtained by adding a peak of unit magnitude at the origin corresponding to the source.

proximately deduced from the data. An analysis of these curves yields widths of ~115° for the PS PSF and ~65° for the PS PSF. These values are each approximately 27.5% greater than the values predicted by the SSA, but their relative values are almost the same, with the PD PSF being 43% narrower than the PS PSF.

B. Multiple Scattering

Imaging environments of practical interest tend not to be single scattering in nature; rather, significant portions of the radiation tend to be multiply scattered before being imaged. The Monte Carlo code used above can be easily modified to demonstrate the results that are due to a multiple-scattering environment. Furthermore, the Rayleigh-scattering function does not usually adequately characterize optical scattering in many media of interest. For a medium such as the milk mixture used in the experiments described in Refs. 7 and 21, where fatty molecules act as the primary scatterers, the Mie-scattering function is typically used in optical scattering simulations.[35] In milk the fat tends to cluster in globules that range in diameter from 0.1 to 20 μm, with an average diameter on the order of 1–3 μm depending on the breed of cow that produced the milk.[39] In the simulation that follows, the Mie solution for particles two free-space wavelengths in radius is used for the scattering function. For more information, see the caption of Figs. 5–7.

The results for a slab of random medium that is four mean free paths thick are shown in Fig. 7 for a medium composed of Mie scatterers. That this multiply scattering Mie medium is more depolarizing than the single-scattering Rayleigh medium is evident in Fig. 7. The x- and z-polarized components transmitted through this multiply scattering Mie medium are close in absolute magnitude, so the corrupting portion of the PD PSF is significantly lower in absolute intensity than is the corrupting portion of the corresponding PS PSF.

4. DISCUSSION AND CONCLUSIONS

The azimuthal width of the portion of the PSF due to scatterers is not the only variable of interest when one is characterizing the overall PSF of the system. The magnitude of the portion of the PSF due to the source relative to the magnitude of the scatterer PSF must also be considered. Notice that the peak intensity of the corrupting portion of the PD PSF is lower than the peak value of the corrupting portion of the PS PSF. The dipole source produces radiation polarized in the $\hat{\mathbf{z}}$ direction only, and hence the portion of the PSF due to the source is identical in PS and PD imaging, so the decreased intensity of the corrupting portion of the PD PSF indicates that the dipole source would become more evident in PD images in scattering media. If the radiation from a particular location on a target were partially polarized, as is often the case in passive imaging with unpolarized illumination,[7,19,21–23] the magnitude of the transmitted peak would be lowered in PDI. This is an important consideration that will help to determine the limits of visibility of partially polarizing target features in scattering media.

The analysis presented here assumes an ideal imaging system (which allows the effects of the scatterers to be isolated), but this assumption is not a limitation. By a suitable alteration of the definition of the intermediate transfer function $G(x_a, y_a)$, Eq. (4) can be directly evaluated. Furthermore, the transfer function can be incorporated into the Monte Carlo simulation to increase the overall fidelity of the model for a particular imaging scheme.

The narrowed portion of the PD PSF can be related to the improved detectability of target features presented by Tyo *et al.*[7] In addition, these results are consistent with the measured PSF and line-spread functions observed by Wang and colleagues in time-resolved PDI.[9,20] The narrowing of the PSF implies that small-scale target features with high-spatial-frequency information (such as edges) can be imaged with greater fidelity by using differential polarimetry in scattering media. It should be noted that the results of Wang and colleagues[9,20] were from experiments conducted at much greater optical thicknesses than the analyses presented here. However, the use of time-resolved imaging in conjunction with PDI allows many of the multiply scattered photons to be eliminated from the PSF by time gating, and PDI is then used to further refine the PSF that is due to the forward-scattered photons.

The initial results presented in this paper help to explain the experimental data that indicate that a system employing PDI is capable of detecting target features through stronger scattering media than is an equivalent polarization-blind imaging system.[7,9,20–23] Topics of further study include generalization of the Monte Carlo model to nonideal imaging systems as well as to the modeling of more-complicated scattering media. The two types of media considered here have well-known properties; however, there are indications that more-complex media such as polydisperse mixtures, chiral scatterers, and optically active host media will have different effects on the deloparization properties of the medium.[22] In addition, only linear PDI of a linearly polarized source was considered here. Investigation of partial polarization, elliptical polarization, and more-general Stokes-vector imaging techniques (such as circular PDI[6,22]) may also provide interesting results that could be useful in certain biomedical and remote sensing applications.

ACKNOWLEDGMENTS

The author thanks N. Engheta, E. N. Pugh, Jr., and M. Rowe for valuable discussions and for their comments on the manuscript.

The author can be reached at the Naval Postgraduate School, Code IW, Room 200A, 589 Dyer Road, Monterey, California 93943-5000, or by phone, 831-656-4476; fax, 831-656-3679; or e-mail, tyo@ieee.org.

REFERENCES AND NOTES

1. B. A. Swartz and J. D. Cummings, "Laser range-gated underwater imaging including polarization discrimination," in *Underwater Imaging, Photography, and Visibility*, R. W. Spinrad, ed., Proc. SPIE **1537**, 42–56 (1991).
2. S. K. Gayen and R. R. Alfano, "Emerging optical biomedical techniques," Opt. Photon. News **7**, 16–22 (March 1996).
3. S. C. W. Hyde, N. P. Barry, R. Jones, J. C. Dainty, and P. M. W. French, "High resolution depth resolved imaging through scattering media using time resolved holography," Opt. Commun. **122**, 111–116 (1996).
4. M. Kempe, W. Rudolph, and E. Welsch, "Comparative study of confocal and heterodyne microscopy for imaging through scattering media," J. Opt. Soc. Am. A **13**, 46–52 (1996).

5. A. Yodh and B. Chance, "Spectroscopy and imaging with diffusing light," Phys. Today **48**, 34–40 (March 1995).
6. G. D. Gilbert and J. C. Pernicka, "Improvement of underwater visibility by reduction of backscatter with a circular polarization technique," in *Underwater Photo Optics I*, A. B. Dember, ed., Proc. SPIE **7**, A-III-1–A-III-10 (1966).
7. J. S. Tyo, M. P. Rowe, E. N. Pugh, Jr., and N. Engheta, "Target detection in optically scattering media by polarization-difference imaging," Appl. Opt. **35**, 1855–1870 (1996).
8. S. G. Demos and R. R. Alfano, "Temporal gating in highly scattering media by the degree of optical polarization," Opt. Lett. **21**, 161–163 (1996).
9. W. B. Wang, S. G. Demos, J. Ali, and R. R. Alfano, "Imaging fluorescent objects embedded inside animal tissues using polarization difference technique," Opt. Commun. **142**, 161–166 (1997).
10. J. F. de Boer, T. E. Milner, M. J. C. van Gemert, and J. S. Nelson, "Two-dimensional birefringence imaging in biological tissue by polarization-sensitive optical coherence tomography," Opt. Lett. **22**, 934–936 (1997).
11. J. M. Harris, "The influence of random media on the propagation and depolarization of electromagnetic waves," Ph.D. dissertation (California Institute of Technology, Pasadena, Calif., 1980).
12. Y. Kuga and A. Ishimaru, "Modulation transfer function and image transmission through randomly distributed spherical particles," J. Opt. Soc. Am. A **2**, 2330–2335 (1985).
13. Y. Kuga and A. Ishimaru, "Modulation transfer function of layered inhomogeneous random media using the small-angle approximation," Appl. Opt. **25**, 4382–4385 (1986).
14. J. W. Goodman, *Introduction to Fourier Optics* (McGraw-Hill, New York, 1968).
15. Q. Ma and A. Ishimaru, "Propagation and depolarization of an arbitrarily polarized wave obliquely incident on a slab of random medium," IEEE Trans. Antennas Propag. **39**, 1626–1632 (1991).
16. C. Brüning, R. Schmidt, and W. Alpers, "Estimation of the ocean wave-radar modulation transfer function from synthetic aperture radar imagery," J. Geophys. Res. C **99**, 9803–9815 (1994).
17. A. Schmidt, V. Wismann, R. Romeiser, and W. Alpers, "Simultaneous measurements of the ocean wave-radar modulation transfer function at L, C, and X bands from the research platform *Nordsee*," J. Geophys. Res. C **100**, 8815–8827 (1995).
18. K. Bhattacharya, A. Ghosh, and A. K. Chakraborty, "Vector wave imagery with a lens masked by polarizers," J. Mod. Opt. **40**, 379–390 (1993).
19. J. S. Tyo, "Polarization difference imaging," Ph.D. dissertation (University of Pennsylvania, Philadelphia, Pa., 1997).
20. S. G. Demos, W. B. Wang, and R. R. Alfano, "Imaging objects hidden in scattering media with fluorescence polarization preservation of contrast agents," Appl. Opt. **37**, 792–797 (1998).
21. M. P. Rowe, E. N. Pugh, Jr., J. S. Tyo, and N. Engheta, "Polarization-difference imaging: a biologically inspired technique for imaging in scattering media," Opt. Lett. **20**, 608–610 (1995).
22. M. P. Silverman and W. Strange, "Light scattering from optically active and inactive turbid media," in *Proceedings of the IS&T/OSA Conference on Optics and Imaging in the Information Age* (Society for Image Science and Technology, Springfield, Va., 1996), pp. 172–180.
23. M. P. Silverman and W. Strange, "Object delineation within turbid media by backscattering of phase-modulated light," Opt. Commun. **144**, 7–11 (1997).
24. A. Ishimaru, *Wave Propagation in Random Media* (Academic, San Diego, Calif., 1978), Vol. 1, Chap. 4.
25. G. E. Anderson, F. Liu, and R. R. Alfano, "Microscope imaging through highly scattering media," Opt. Lett. **19**, 981–983 (1994).
26. M. Gu, T. Tannous, and J. R. Sheppard, "Effect of an annular pupil on confocal imaging through highly scattering media," Opt. Lett. **21**, 312–314 (1996).
27. The apertures can be projected onto the intermediate plane without changing the results as long as the extent of the object is much smaller than the projected size of the limiting aperture of the system. When this condition is met, the vignetting can be ignored (see Ref. 14, chap. 5).
28. For simplicity, the host medium in which the scatterers are embedded is assumed to be free space, although in general it is some other medium.
29. $\vec{\mathbf{E}}_{sc}(\hat{\mathbf{s}})$ must fall off as $1/r$ as one travels along the direction $\hat{\mathbf{s}}$; the formulation in Eq. (2) gives the relative amplitude scattered in any direction at some constant distance from the scatterer. The $1/r$ fall-off will be taken into account, along with the system parameters, in the analysis that follows.
30. J. A. Stratton, *Electromagnetic Theory* (McGraw-Hill, New York, 1941), Chaps. 7 and 9.
31. $\hat{\mathbf{r}}$ and $\hat{\boldsymbol{\theta}}$ refer to the spherical unit vectors at the position $\hat{\mathbf{r}}_n$ with respect to the Cartesian coordinate system shown in Fig. 2.
32. Strictly speaking, Eq. (12) does not follow directly from Eq. (11). Equation (11) states that there is an ideal E-field point source given by $\kappa^2\vec{\mathbf{E}}\delta(x_f + x_n)\delta(z_f + z_n)$. This source can also be thought of as an ideal intensity point source given by $\kappa^2|\vec{\mathbf{E}}|^2\delta(x_f + x_n)\delta(z_f + z_n)$.
33. The term polarization sum was introduced in Ref. 21. It is meant to differentiate between a true, polarization-blind image where intensity alone is measured and a sum image formed by adding the intensities obtained at orthogonal polarizations. The two concepts are completely equivalent, and the term PS image is retained to provide the reader with information concerning how a specific image was formed.
34. L. G. Henyey and J. L. Greenstein, "Diffuse radiation in the galaxy," Astrophys. J. **93**, 70–83 (1941).
35. M. J. C. van Gemert, S. L. Jacques, H. J. C. M. Sterenborg, and W. M. Star, "Skin optics," IEEE Trans. Biomed. Eng. **36**, 1146–1154 (1989).
36. L. L. Carter and E. D. Cashwell, *Particle Transport Simulation with the Monte-Carlo Method* (Technical Information Center, Energy Research and Development Association, Oak Ridge, Tenn., 1975).
37. B. R. Frieden, *Probability, Statistical Optics, and Data Testing*, 2nd ed., (Springer-Verlag, New York, 1991), Chap. 7.
38. This experiment investigates the PSF that is due to a linearly polarized source. The portion of the radiation that is unpolarized will not be imaged by PDI.
39. L. M. Lampert, *Modern Dairy Products* (Chemical Publishing Co., New York, 1965).